

The influence of surface CO_2 condensation on the evolution of warm and cold rocky planets orbiting Sun-like stars

I. Bonati,^{1*} R. M. Ramirez,^{1,2}

¹Earth-Life Science Institute, Tokyo Institute of Technology, Tokyo, Japan

²Space Science Institute, Boulder, Colorado, USA

Accepted 2021 March 19. Received 2021 March 17; in original form 2020 April 13.

ABSTRACT

The habitable zone is the region around a star where standing bodies of liquid water can be stable on a planetary surface. Its width is often assumed to be dictated by the efficiency of the carbonate-silicate cycle, which has maintained habitable surface conditions on our planet for billions of years. This cycle may be inhibited by surface condensation of significant amounts of CO_2 ice, which is likely to occur on distant planets containing high enough levels of atmospheric CO_2 . Such a process could permanently trap CO_2 ice within the planet, threatening its long-term habitability. Recent work has modeled this scenario for initially cold and icy planetary bodies orbiting the Sun. Here, we use an advanced energy balance model to consider both initially warm and cold rapidly-rotating planets orbiting F - K stars. We show that the range of orbital distances where significant surface CO_2 ice condensation occurs is significantly reduced for warm start planets. Star type does not affect this conclusion, although surface CO_2 ice condenses over a larger fraction of the habitable zone around hotter stars. The warm start simulations are thus consistent with 1-D model predictions, suggesting that the classical habitable zone limits in those earlier models are still valid. We also find that the cold start simulations exhibit trends that are consistent with those of previous work for the Sun although we now extend the analysis to other star types.

Key words: planets and satellites: terrestrial planets – planets and satellites:atmosphere – planets and satellites: physical evolution

1 INTRODUCTION

During the course of its evolution, Earth is thought to have exhibited mostly warm surface conditions that were temporarily interrupted by a few sporadic cooling episodes, triggered by processes taking place in its interior, atmosphere, and host star. The resultant climatic changes can manifest as mild oscillations, or even as extreme snowball events capable of engulfing Earth’s entire surface in ice (Kirschvink 1992; Hoffman et al. 1998). Nevertheless, the carbonate-silicate cycle, which maintains the balance of atmospheric CO_2 between the atmosphere and the interior, has allowed Earth to escape permanent glaciation and maintain clement surface conditions throughout time (Hoffman et al. 1998).

However, large amounts of atmospheric CO_2 on a cold enough planet, as is the case for some depictions of early Mars (Kasting 1991; Wordsworth et al. 2013), can have a detrimental effect on its habitability. A number of recent studies (Kasting 1991; Pierrehumbert 2005; Pierrehumbert et al. 2011; Forget et al. 2013; Soto et al. 2015; Turbet et al. 2017; Kadoya & Tajika 2019) have shown that once CO_2 partial pressures exceed the saturation level, and sur-

face temperatures are low enough, significant condensation of CO_2 ice can occur at the poles (Figure 1). The relatively high Rayleigh scattering of CO_2 , along with the resultant increase in the planetary albedo, work to enhance the ice-albedo feedback (Kasting 1991) and keep the planet cold. Moreover, the high density of CO_2 ice compared to water ice can lead to surface condensation and subsurface sequestration of the former, removing some CO_2 from the atmosphere forever. This could result in a permanently glaciated state and prevent planets from achieving warm states. In that case, the influence of the carbonate-silicate cycle in sustaining habitability is greatly lessened, if not gone altogether (Turbet et al. 2017).

While the carbonate-silicate cycle has stabilized surface temperatures over time on Earth, this might not be the case for bodies orbiting other stars and/or located at different orbital distances, and having different atmospheric CO_2 inventories. In particular, CO_2 pressures at large orbital distances are high enough for surface condensation and Rayleigh scattering to counter the greenhouse effect, directly impacting the width of the classical CO_2 - H_2O habitable zone (Kasting et al. 1993; Kopparapu et al. 2013; Ramirez 2018). It is therefore important to assess the role of CO_2 in determining a given planet’s fate. Turbet et al. (2017) have recently addressed this issue by using a 3-D Global Climate Model (GCM) to simulate the

* E-mail: irene.bonati@elsi.jp (IB)

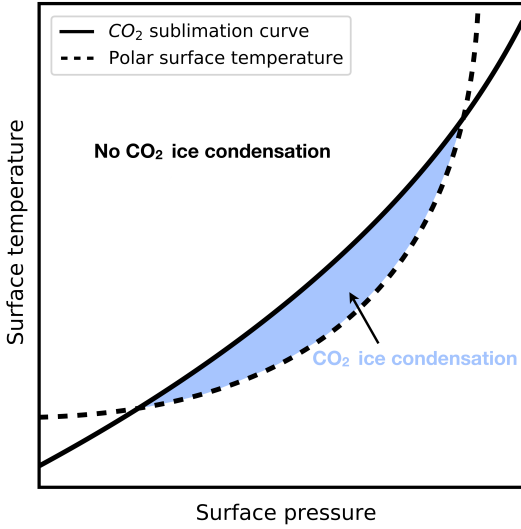


Figure 1. Schematic representation showing the CO_2 sublimation and the polar surface temperature curves as a function of surface temperature and pressure. At the poles, the surface temperature is low enough to drop below the CO_2 sublimation temperature. The presence of a sufficiently high amount of atmospheric CO_2 can, in turn, drive precipitation of CO_2 ice onto the planetary surface. Such a phenomenon is less likely to happen for a small atmospheric CO_2 inventory or when the greenhouse effect of CO_2 dominates at sufficiently high surface pressures. Adapted from Figure 1 of Soto et al. (2015).

evolution of terrestrial planets across the habitable zone, and concluded that bodies initially assumed to be fully frozen remained that way, exhibiting permanent surface CO_2 ice condensation at orbital distances as small as ~ 1.27 AU from the Sun for an atmospheric CO_2 pressure of 1 bar. In comparison, 1-D calculations suggest that the habitable zone extends to ~ 1.47 AU at that CO_2 pressure level (Kasting et al. 1993; Kopparapu et al. 2013; Ramirez 2018). All of this suggests that CO_2 condensation in more advanced climate modeling simulations may have an even more detrimental effect on planetary habitability than previously calculated, possibly decreasing the size of the habitable zone as compared to 1-D modeling simulations.

Turbet et al. (2017) had simulated planets with initially fully-glaciated surface conditions (cold start worlds) orbiting the Sun. In contrast, habitable-zone planets that start their evolution warm (warm start worlds) may exhibit a different response to CO_2 condensation. Here, we employ an advanced energy balance model (EBM) to investigate the parameter space of surface CO_2 condensation for cold and warm rotating planets with different atmospheric CO_2 pressures orbiting Sun-like (F - K) stars. We compare the cold and warm start results and discuss implications for the width of the habitable zone.

2 METHODS

2.1 Governing equations

We make use of an advanced non-grey energy balance model (EBM), similar to that described in Ramirez & Levi (2018) and Ramirez (2020), which is itself based on other similar models (see also North & Coakley Jr (1979), North et al. (1981), Williams & Kasting (1997), and Vladilo et al. (2013)) to determine the presence of CO_2 ice condensation and its influence on the fate of bodies

orbiting Sun-like stars. We study the evolution of Earth-like planets assuming cold ($T_{\text{surf}}=230$ K) or warm ($T_{\text{surf}}=280$ K) starts. The EBM is coupled to a 1-D radiative-convective climate model that provides the radiative transfer calculations. The reader is redirected to Ramirez (2020) for a more detailed explanation of the model, but we reiterate some of the key details here.

The present model follows the radiative energy balance principle (e.g., Williams & Kasting 1997), according to which planets in thermal equilibrium radiate as much energy to space as they receive from their host star. The atmospheric-ocean energy balance is expressed as (e.g., James & North 1982; Williams & Kasting 1997; Batalha et al. 2016):

$$C_p \frac{\partial T(x,t)}{\partial t} - \frac{\partial}{\partial x} D (1-x^2) \frac{\partial T(x,t)}{\partial x} + I - L \left(\frac{dM_{\text{col},CO_2}}{dt} \right) = S(1-A), \quad (1)$$

where C_p is the effective heat capacity, T is the zonally averaged surface temperature, x is the sine of the latitude, t is time, D is the heat diffusion coefficient (i.e., the latitudinal transport of heat), I is the outgoing infrared flux to space, S is the absorbed fraction of incident solar flux, L is the latent heat flux per unit mass of CO_2 ($5.9 \cdot 10^5$ J/kg; Forget et al. (1998)), M_{col,CO_2} is the column mass of CO_2 which sublimates from or condenses onto the planetary surface, and A is the albedo at the top of the atmosphere. Equation 1 is solved for every time step using a second-order finite difference scheme.

The modeled planets are Earth-sized and are subdivided into 36 five degree wide latitudinal belts with land and ocean coverage similar to present-day Earth (i.e., 70% oceans and 30% land). Flat topography is assumed for simplicity. Planets are in circular orbits and the length of day is 24 hours. As per Turbet et al. (2017), we assume that volcanic outgassing rates at a given stellar flux are always high enough to support stable climates. Thus, our worlds do not undergo limit cycles, which lead to hypothetical oscillations between warm and cold climates for planets with low volcanic outgassing rates (Haqq-Misra et al. 2016; Paradise & Menou 2017; Kadoya & Tajika 2019). We note that the existence of limit cycles is controversial and is based on various weathering and surface albedo assumptions that may not be applicable in many circumstances (Ramirez 2017; Graham & Pierrehumbert 2020).

Our calculations assume that atmospheres are fully-saturated and consist of 1 bar N_2 for a range of atmospheric CO_2 pressures. The thermal diffusion coefficient D is calculated using the scaling relation (with the subscript "0" referring to present Earth values):

$$\left(\frac{D}{D_0} \right) = \left(\frac{p}{p_0} \right) \left(\frac{C_p}{C_{p0}} \right) \left(\frac{m_0}{m} \right)^2 \left(\frac{\Omega_0}{\Omega} \right)^2 \left(\frac{T_{\text{surf,ave}}}{T_0} \right)^{12}, \quad (2)$$

where $D_0 = 0.58 \text{ Wm}^{-2}\text{K}^{-1}$, $C_{p0} = 10^3 \text{ g}^{-1}\text{kgK}^{-1}$, p is the atmospheric pressure ($p_0 = 1$ bar), m is the atmospheric mass ($m_0 = 28 \text{ kg}$), Ω is the planetary rotation rate ($\Omega_0 = 7.27 \cdot 10^{-5} \text{ rads}^{-1}$), and $T_{\text{surf,ave}}$ is the annual average surface temperature ($T_0 = 288 \text{ K}$). A crude temperature dependence is added to this equation to simulate the importance of latent heat release and transport at high temperatures (Caballero & Langen 2005; Rose et al. 2017). The exponent 12 on the right side of Equation 2 gives the right latitudinal temperature structure in comparing our results to those of Figure 1 from Turbet et al. (2017), which displays an average temperature $T_{\text{surf,ave}} \sim 225 \text{ K}$. Without this temperature dependence, equator-pole temperature gradients are underestimated and heat transport is overestimated at cold temperatures.

The model is able to distinguish between land, ocean, ice, and clouds. As the atmosphere warms near and above the freezing point, water clouds form, with the latitudinal cloud coverage (c) dictated by:

$$c = \min \left(0.72 \log \left(\frac{F_C}{F_E} + 1 \right), 1 \right). \quad (3)$$

Here, F_C is the convective heat flux, F_E is the convective heat flux for the Earth at 288 K ($\sim 90 \text{ W/m}^2$). This equation is similar to that used in the Community Atmosphere Model (CAM) GCM (Xu & Krueger 1991; Yang & Abbot 2014) and yields an Earth-like cloud coverage $c \sim 50\%$ at a mean surface temperature of 288 K. For simplicity, cloud decks do not overlap [], and an averaged cloud fraction is computed at each latitude. This is an improvement over 1-D models that place such clouds at the surface (Kasting et al. 1993; Kopparapu et al. 2013).

The CO₂ clouds modeled here are non-absorbing, and thus radiatively inactive. This is consistent with recent simulations suggesting that their greenhouse effect may be very small in these dense CO₂ atmospheres (Kitzmann 2016). Even so, our CO₂ clouds still impact the planetary albedo, affecting planetary surface temperatures and CO₂ precipitation. Following GCM predictions (Forget et al. 2013), a cloud coverage $c = 50\%$ is assumed for CO₂. Such clouds form once temperatures along the adiabat are cold enough for CO₂ to condense. Following (Williams & Kasting 1997) we assume that all CO₂ clouds form in that layer.

For each time step, spanning about 2 hours of a planet’s evolution, the new average surface temperature is updated for every latitude belt following Equation 1, along with the resulting H₂O and CO₂ inventories in the atmosphere and surface. The model simulates the entire year, including seasons, using an explicit forward marching numerical scheme to achieve convergence. Such convergence is reached when the average annual surface temperature does not change by more than $\sim 0.1 \text{ K}$ and both CO₂ condensation and sublimation rates are balanced.

To validate our model, we compute the northward heat flux for a planet with 330 ppm CO₂ (i.e., similar to present Earth) that orbits the Sun at 1 AU at different obliquities by using the following expression:

$$\mathcal{F}_\lambda = 2\pi R \cos \lambda F_\lambda = 2\pi R^2 D \cos^2 \lambda \frac{\partial T}{\partial x}, \quad (4)$$

where \mathcal{F}_λ is the latitudinal energy transport per unit length, R is the planetary radius, λ is the latitude (between -90° and 90° , and $\frac{\partial T}{\partial x}$ is the temperature gradient between different latitude belts. The obtained flux, shown in Figure 2, matches well with similar models used in past studies (e.g., Williams & Pollard 2003).

At the start of the final orbit (after convergence is achieved), we track how much surface CO₂ condenses into ice, melts, or sublimates at a given latitude and time step. This approach provides a consistent comparison between warm and cold start scenarios. The phase curve of CO₂ employed in this model uses established data parameterized from previous 1-D radiative-convective climate models (Kasting 1991) and matches very well with modern data (Fray & Schmitt 2009). CO₂ ice forms at cold enough surface temperatures and when the saturation pressure is reached. The albedo of surface CO₂ ice (dry ice) in our model is 0.6 (Warren et al. 1990), which is the same value used in Turbet et al. (2017).

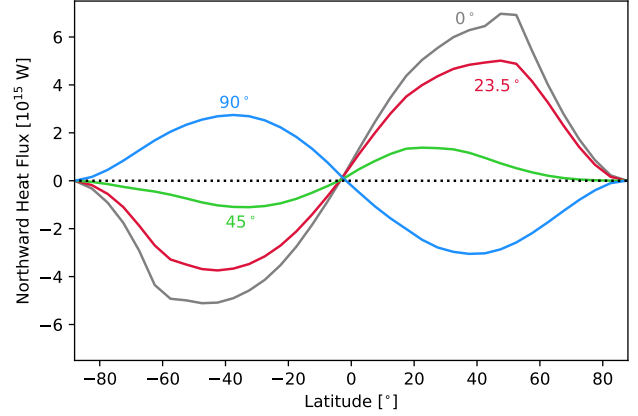


Figure 2. Meridional heat flow for an Earth-like planet orbiting a Sun-like star at 1 AU, having an atmospheric pressure of CO₂ of $3.3 \cdot 10^{-4}$ bar and obliquities 0°, 23.5°, 45°, and 90°. At low obliquities, heat is transported from the equator towards the poles, while transport in the opposite direction is favored at high enough obliquities.

Table 1. Initial conditions for planets starting out cold and warm.

Parameter	Cold start	Warm start
Surface temperature T_{surf} [K]	230	280
H ₂ O cloud fraction $c_{\text{H}_2\text{O}}$	0	0.26
CO ₂ cloud fraction c_{CO_2}	0	0
Land snow fraction	1	0.5

2.2 Initial conditions and parameter space

We model the evolution of Earth-sized bodies, orbiting F0, K5, and solar (G2) stars. We vary the initial CO₂ atmospheric pressure, surface temperature (cold and warm start), planetary obliquity, and semi-major axis. The initial conditions are summarized in Table 1. If a planet starts out cold, there are initially no water clouds in the atmosphere. The global surface temperature is set to $T_{\text{surf}} = 230 \text{ K}$, and the land snow fraction is equal to 1 (i.e., the continents are fully covered in ice). This was done to approximate the initial conditions of Turbet et al. (2017).

On the other hand, if a planet starts out warm, the surface temperature is set to $T_{\text{surf}} = 280 \text{ K}$, with a land snow fraction of 0.5. The fractional cloud cover from water vapor is $c_{\text{H}_2\text{O}} = 0.26$ (resulting from Equation 1). There are no CO₂ clouds in the initial step for either case (i.e., $c_{\text{CO}_2} = 0$). These starting conditions are meant to approximately simulate the modeling conditions of Turbet et al. (2017). However, after the initial step, both cloud coverage and surface temperatures are calculated self-consistently.

We explore different parameters as shown in Table 2. We do not simulate planets located at larger semi-major axis distances than those showed in Table 2 because modeled surface temperatures at these CO₂ pressures are below what is possible for our radiative transfer model ($T_{\text{surf}} = 150 \text{ K}$). Nevertheless, the sampled parameter space is more than sufficient to obtain the overall trends.

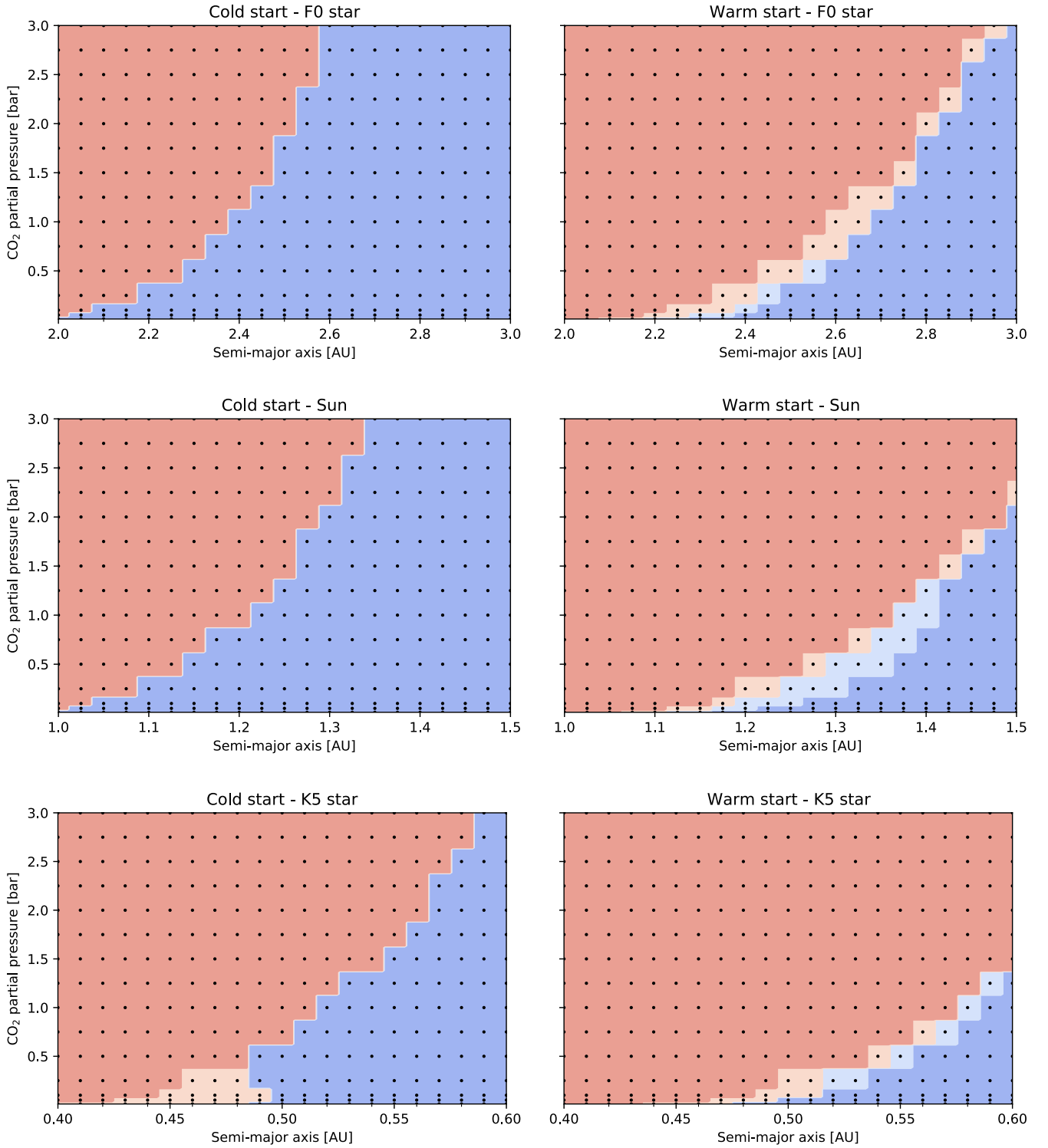


Figure 3. Steady-state solutions reached by warm start (ice-free body) and cold start (fully-glaciated body) planets orbiting F0, Sun-like, and K5-type stars as a function of orbital distance (in AU) and initial atmospheric CO_2 partial pressure. The modeled planets have an Earth-like continental fraction and an obliquity of 23.5° . The dark and light red regions comprise bodies that are ice-free and partially (or fully) covered in H_2O ice, respectively. The light and dark blue regions represent partially (or fully) ice-covered and snowball planets, respectively, exhibiting both H_2O and CO_2 ice on their surfaces. Note: The horizontal scale is different for each host star. Our model predicts similar trends at 0° obliquity (not shown).

Table 2. Parameter space investigated in the simulations.

Parameter	Values		
CO_2 partial pressure range [bar]	0.01-3.0		
Obliquity [°]	0, 23.5		
	<u>F0 star</u>	<u>Sun</u>	<u>K5 star</u>
Stellar temperature [K]	7200	5800	4400
Stellar mass [M_{\odot}]	1.5	1.0	0.6
Stellar luminosity [L_{\odot}]	4.3	1.0	0.15
Semi-major axis range [AU]	2.0-3.0	1.0-1.5	0.4-0.6

3 RESULTS

3.1 Steady-state climate regimes

We allow the CO_2 partial pressure to evolve until CO_2 sublimation and condensation rates are balanced. Figure 3 shows the steady-state climate regimes obtained for initially cold and warm Earth-sized bodies having an obliquity of 23.5° and orbiting different types of stars (solar twin-G2, as well as F0 and K5 stars), as a function of their orbital distance and initial atmospheric CO_2 pressure. We distinguish between four final scenarios (Figure 3).

As expected, surface CO_2 ice condensation starts occurring at smaller orbital distances for cold start planets (left panels in Figure 3) as compared to bodies that start out warm (right panels in Figure 3). For the solar case, the 1 bar CO_2 cold start scenario exhibits surface CO_2 ice condensation starting from orbital distances as small as ~ 1.22 AU, which compares favorably to the ~ 1.27 AU value found by Turbet et al. (2017). The equivalent distances for the F0 and K5 stars are ~ 2.4 AU and ~ 0.52 AU, respectively. In contrast, surface CO_2 ice condensation for warm starts does not occur until ~ 1.37 AU for the 1 bar CO_2 solar case, 0.15 AU farther out than for the cold start scenario. At this same pressure level, CO_2 surface ice starts forming at ~ 2.7 AU and ~ 0.58 AU for the F0 and K5 stars, respectively. This is about 0.3 AU and 0.06 AU farther out than for the equivalent cold start cases. For comparison, 1-D radiative-convective climate modeling simulations predict that planets with a 1 bar CO_2 atmosphere orbiting F0, solar, and K5 stars can display habitable surface conditions at distances as far as ~ 2.75 , 1.47, and 0.58 AU, respectively (Kasting et al. 1993; Kopparapu et al. 2013; Ramirez 2018), assuming the luminosity values given in Table 2. These values are only slightly farther out than the most distant extent of the red regions at the 1 bar level (Figure 3). Although nearly the same size, the warm regions in the warm starts still span slightly smaller areas (generally) than predicted in 1-D radiative-convective climate modeling simulations (Kasting et al. 1993; Kopparapu et al. 2013; Ramirez 2018). This is because of the EBM’s increased ice-albedo feedback.

The distances beyond which surface CO_2 ice condensation starts forming are pressure-dependent, as a result of the greenhouse effect of CO_2 . At higher pressures, surface CO_2 ice condensation in both warm and cold start cases occurs farther away from the host star, whereas the opposite occurs at lower pressures. Moreover, we find that the surface CO_2 ice condensation encompasses a larger region for the hotter stars (alternatively, the dark and light red areas are larger for cooler stars). This is because near-infrared absorption is lower and Rayleigh scattering is higher for planetary atmospheres orbiting hotter stars, cooling the planet and causing CO_2 surface ice condensation to occur closer to the star.

A key observation from our cold starts is that a planet cannot escape full glaciation for orbital distances exceeding ~ 2.6 , ~ 1.33 , and ~ 0.59 AU for the F0, solar, and K5 star cold start scenarios

(Figure 3). In these cases, the planet remains glaciated with surface CO_2 ice condensation regardless of the atmospheric CO_2 content. This difference is attributed to the weaker heat transport and higher surface albedo associated with such cold starts. Although Turbet et al. (2017) does not necessarily obtain CO_2 surface ice in all of these cases, in agreement with our model, they predict snowball states.

3.2 Latitudinal variation of surface temperature and amount of surface CO_2 ice

The surface temperatures during the last orbit are illustrated in Figure 4 as a function of latitude, for both initially cold and warm planets having an initial atmospheric CO_2 pressure of 1 bar and obliquities of 23.5° and 0° . These planets are located at intermediate orbital distances from the host star, close to the transition between ice-free and fully ice-covered bodies (see Figure 3). At such semi-major axes (and intermediate atmospheric CO_2 pressures), the initial state of a planet (warm or cold) is a strong predictor of the final state of the planet. For instance, warm start planets tend to end up warm as well. Likewise, a cold start planet at these distances converges to a frozen solution. In contrast, at smaller orbital distances, the intense starlight produces warm planets regardless of the starting state. At larger semi-major axes, the reduction in starlight, combined with more intense surface CO_2 condensation, favors cold solutions (Figure 3).

Low obliquity bodies receive more direct insolation at the equator, which causes large temperature differences between the latter and the poles, as well as generally lower polar surface temperatures. This also produces the tendency for equatorial surface temperatures to be higher at 0° than at 23.5° obliquities, especially at higher CO_2 pressures. For intermediate atmospheric CO_2 pressures, this could imply slightly more surface CO_2 ice at higher (23.5°) obliquity. For example, the fraction of atmospheric CO_2 that precipitates onto the planetary surface of planets having an initial atmospheric CO_2 pressure of 1 bar is $\sim 93.1\%$ (0° obliquity) and $\sim 95.8\%$ (23.5° obliquity) for bodies orbiting F0 stars, $\sim 60.4\%$ (0° obliquity) and $\sim 75.1\%$ (23.5° obliquity) for planets surrounding the Sun. Soto et al. (2015) also found a similar trend at these intermediate CO_2 pressures. We attribute this to the decreased heat transport in the winter hemisphere, which favors surface CO_2 ice formation at the winter poles for these moderately dense atmospheres. For example, meridional heat exchange to the poles is greater at low obliquity than it is to the northern pole during southern summer at high obliquity. This is because the northern pole is farther away from the sub-stellar point (during southern summer) in the high obliquity scenario, producing colder seasonal minimum temperatures. Likewise, seasonal temperatures at the southern pole are at a maximum. The opposite thought experiment holds true for northern summer. Nevertheless, this trend breaks in our model for bodies orbiting K5 stars, with greater condensation at low obliquity: $\sim 16.5\%$ (0° obliquity) and $\sim 10.6\%$ (23.5° obliquity) (Figure 4). Moreover, like the results by Soto et al. (2015) for the Sun, the trends reverse and our model predicts slightly more surface ice formation at low CO_2 pressures (as low as 0.01 bar; not shown) for the low obliquity solar and F0 cases. Again, the K5 case exhibits the opposite trend, with more surface ice production at high obliquity in that scenario. This discrepancy may be related to differences in the amount of near-infrared emission among the star types. The addition of topography would further complicate these trends, creating cold traps that favor CO_2 condensation beyond what is predicted in the flat topography worlds considered here (Forget et al. 2013; Wordsworth et al. 2013).

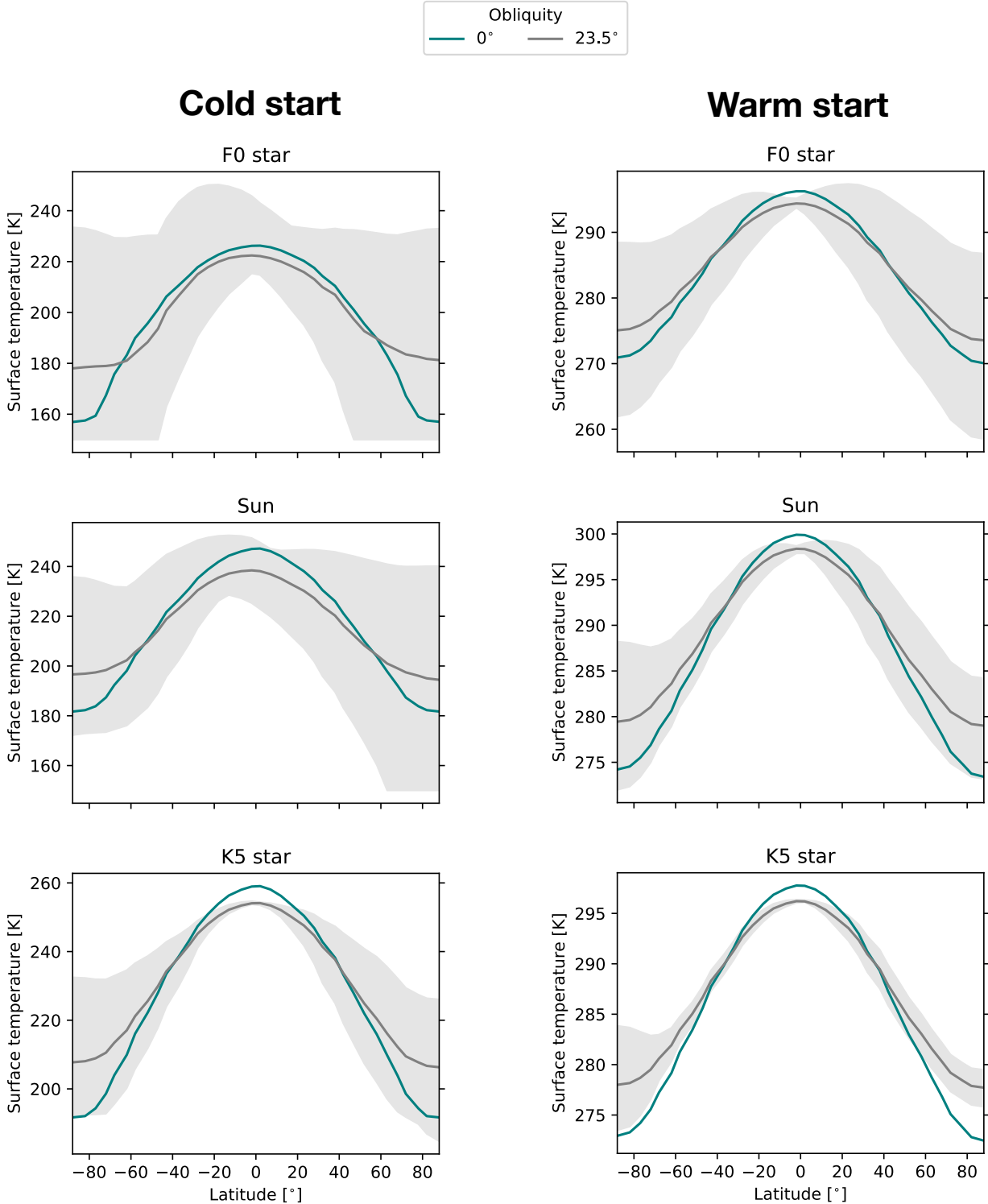


Figure 4. Latitudinally averaged annual surface temperature profiles for cold start (initial $T_{\text{surf}} = 230$ K; left column) and warm start (initial $T_{\text{surf}} = 280$ K; right column) planets with an initial atmospheric CO_2 pressure of 1 bar for both 0° (dark green) and 23.5° (grey) obliquity cases orbiting F0, K5, and Sun-like stars at 2.5 AU, 0.53 AU, and 1.25 AU, respectively. Solid lines represent mean annual surface temperatures, and the shaded regions comprise the amplitude of variation between the minimum and maximum annual surface temperatures for 23.5° obliquity. In contrast, 0° obliquity planets experience no seasonal variability. Warm start planets (right column) always have an atmospheric CO_2 pressure of 1 bar. For fully glaciated planets (left column) the annual average amounts of atmospheric CO_2 are $6.91 \cdot 10^{-2}$ bar (0°) and $4.22 \cdot 10^{-2}$ bar (23.5°) for bodies orbiting F0 stars, $3.96 \cdot 10^{-1}$ bar (0°) and $2.49 \cdot 10^{-1}$ bar (23.5°) for planets orbiting Sun-like stars, and $8.35 \cdot 10^{-1}$ bar (0°) and $8.94 \cdot 10^{-1}$ bar (23.5°) for planets orbiting K5 stars. The remaining CO_2 condenses on the planetary surface as ice. Seasonal ice may persist at the end of the model year, which is the close of southern winter. The model does not compute latitudinal temperatures below $T_{\text{surf}} = 150$ K, although calculated surface temperatures are mostly above that threshold. The few cases that do not are seasonal minimum temperatures that do not significantly impact average temperatures or computed trends.

We also find that the amount of condensed surface CO_2 at a given equivalent distance (e.g., similar flux level) is highest for planets orbiting F0 stars and lowest for worlds around K5 stars (Figure 4). This is because planets orbiting cooler stars exhibit less Rayleigh scattering and enhanced near-infrared absorption, both of which enhance warming (Kasting et al. 1993). This suggests that planets orbiting cooler stars may be more resistant against atmospheric collapse.

3.3 Fraction of condensed CO_2 ice

As shown by the Mars simulations of Soto et al. (2015), the fraction of atmospheric CO_2 that condenses onto a planetary surface depends heavily on the initial atmospheric CO_2 pressure. The fraction of atmospheric CO_2 lost to the surface as a function of orbital distance and starting atmospheric CO_2 pressure is shown in Figure 5. The obtained trends reflect the competition between cooling (CO_2 ice condensation, clouds, and Rayleigh scattering) and warming (greenhouse effect, stellar insolation) processes.

We obtain fractions of condensed atmospheric CO_2 ranging between $\sim 1\%$ and more than 90%. The largest amounts of condensed CO_2 are obtained for cold planets located at large orbital distances (e.g., reduced insolation). We note that at the lowest atmospheric CO_2 pressures (i.e., smaller than 0.05 bar) saturation is not reached as easily, and atmospheric CO_2 precipitates in smaller amounts (between 1 and 10%, Figure 5). Similarly, at high enough atmospheric CO_2 pressures, the greenhouse effect dominates, countering surface ice condensation, especially at equatorial latitudes. In particular, it is the enhanced warming from CO_2 - CO_2 collision-induced absorption at higher pressures that offsets such atmospheric losses (Wordsworth et al. 2010; Ramirez et al. 2014). However, while high initial CO_2 pressures can decrease the magnitude of condensation at small orbital distances, atmospheric collapse occurs throughout most or even the whole CO_2 pressure range explored here for planets on larger orbits.

Even though the orbital and pressure range at which CO_2 condensation takes place is larger for planets that begin their evolution cold (see also Figure 3), we find that the transition towards collapse ($> 10\%$ atmospheric CO_2 condensation) generally occurs more abruptly for warm start planets (Figure 5). This is related to the orbital distance at which CO_2 first starts to condense. For the cold start cases, the onset of CO_2 condensation occurs closer to the host star, where more insolation is available to counter this process, slowing down the transition to collapse. In contrast, atmospheric CO_2 condensation initiates at large orbital distances for warm start planets, where there is less stellar energy to counter condensation.

4 DISCUSSION

4.1 Implications for planetary habitability on early Mars, Earth, and exoplanets

In agreement with Turbet et al. (2017), our model finds that CO_2 surface condensation can be a detriment to the habitability of cold start planets (Figure 3). As the dense surface CO_2 ice becomes sequestered within the subsurface, the atmospheric CO_2 pressure decreases, which promotes even more ice formation, possibly leading to atmospheric collapse (Turbet et al. 2017). Unlike Earth, where volcanism ended snowball episodes (Hoffman et al. 1998), it might be more difficult for distant cold planets to avoid permanently glaciated conditions. This is because once CO_2 pressures exceed

saturation, CO_2 is increasingly removed from the atmosphere before temperatures ever become warm enough. An exception to this could be volcanism rich in H_2 or CH_4 , which could produce sufficient CO_2 - H_2 or CO_2 - CH_4 collision-induced absorption at high enough concentrations (percent level) and CO_2 pressures (Ramirez et al. 2014; Wordsworth et al. 2017; Ramirez & Kaltenecker 2017, 2018; Turbet et al. 2019). Nevertheless, cold start planets that are close enough to their stars receive enough energy to circumvent the above problems (Figure 3).

The above provides some interesting implications. A number of studies argue that Mars (located at 1.52 AU) was a cold planet that had undergone numerous transient warming episodes over geologic timescales, possibly aided by supplementary volcanic gases or other mechanisms in a predominantly CO_2 atmosphere (Wordsworth et al. 2013; Batalha et al. 2016; Wordsworth et al. 2017; Kite et al. 2020; Hayworth et al. 2020). However, multiple sporadic warming episodes would be very difficult to achieve in practice because the excess CO_2 will be removed from the atmosphere once a warm period ends. This will not only enhance the ice-albedo feedback, raising the planetary albedo and triggering atmospheric collapse, but the atmospheric CO_2 would be gradually removed from the atmospheric-surface system forever as it sinks below the less dense H_2O ice. Some estimates of the early water inventory suggest that early Mars could have had a global equivalent water layer that was at least a couple of hundred meters deep (Villanueva et al. 2015; Ramirez et al. 2020). This would have been a sufficiently large reservoir to absorb much of the condensing surface CO_2 , decreasing the likelihood of subsequent transient warming episodes (Turbet et al. 2017).

In the case of limit cycles for instance, models often assume dirty low albedo (0.35) surface CO_2 ice (Batalha et al. 2016; Kadoya & Tajika 2019; Hayworth et al. 2020). This helps increase the absorbed stellar flux, which favors deglaciation and the occurrence of limit cycles. However, observations suggest that the mean CO_2 ice albedo on present Mars is much higher (Forget et al. 2013). Therefore, assuming such a low albedo on a global scale may be unrealistic. Also, limit cycle models almost always assume a linear relationship between weathering rate and dissolution of [H+] in groundwater (Batalha et al. 2016; Kadoya & Tajika 2019; Hayworth et al. 2020). However, experiments have shown that this relationship is much weaker for real silicate rocks (Asolekar et al. 1991), greatly reducing the occurrence of limit cycles (Ramirez 2017). Thus, it is not clear if such global episodic warm episodes had ever occurred on early Mars, at least during the climate optimum of maximum fluvial incision. If they did, they may have been very few in number.

In contrast to our cold start cases, our warm start simulations suggest that the condensation of surface CO_2 ice affects a much smaller range of orbital distances. Irrespective of the star type, the range of semi-major axes and CO_2 pressures for which planets exhibit habitable surface conditions is similar to that predicted by 1-D calculations of the habitable zone (Kasting et al. 1993; Ramirez 2018). Warm start cases that are distant enough to manifest significant surface CO_2 condensation suffer the same habitability problems discussed above for cold start planets. These results also have implications for our own planet. The Earth, by definition, is located close enough to the star where surface CO_2 ice condensation is impossible under normal circumstances (Figure 3), and it would have been warm so long as the greenhouse effect, including from CO_2 , was potent enough. Nevertheless, the Hadean Earth likely had a CO_2 -rich atmosphere (Kasting 2014), suggesting that it was almost certainly a warm start planet, possibly facilitating an early emergence of life.

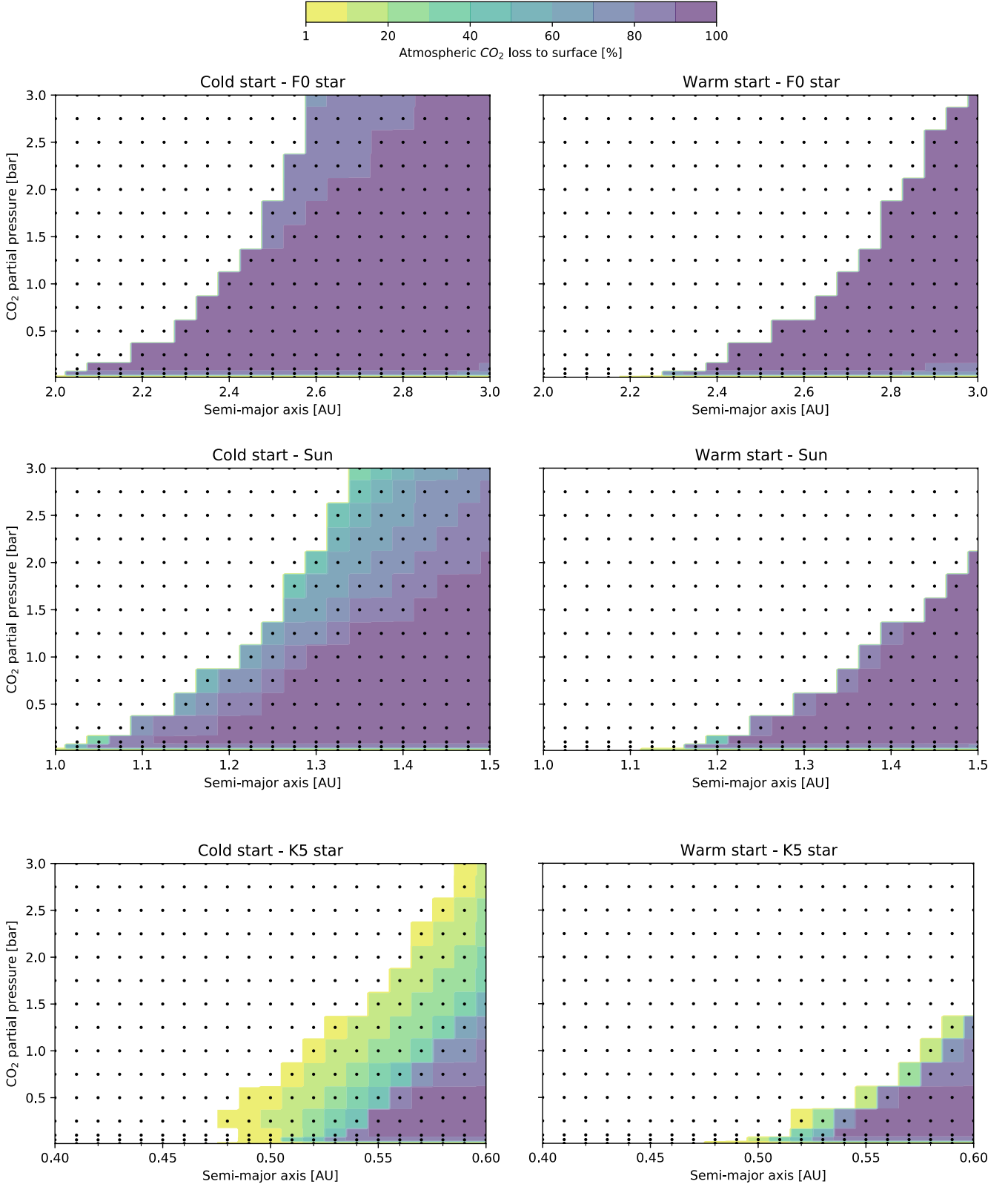


Figure 5. Fraction of atmospheric CO_2 condensed on planetary surface as a function of orbital distance (in AU) and initial atmospheric CO_2 pressure for cold start (left column) and warm start (right column) planets orbiting F0 (upper row), Sun-like (middle row) and K5 (lower row) stars. The obliquity is 23.5° . White regions denote parameter combinations for which no CO_2 ice condensation is observed (see also Figure 3).

4.2 Comparison with previous studies

Although we obtain similar trends, our cold start results differ in certain respects from those of [Turbet et al. \(2017\)](#). In particular, there are discrepancies in the spatial coverage of the red (ice-free or ice-covered planets with no *CO₂* ice) and blue (cold and icy planets displaying surface *CO₂* ice) colored regions in [Figure 3](#) between the two studies, which are likely to be mostly attributed to model differences (although there are slight differences in definition of the regions as well). In particular, EBMs such as this one are quite sensitive to the ice-albedo feedback, and are thus more prone to abrupt transitions between cold and warm climate states ([Ramirez & Levi 2018](#)), as shown in [Figure 3](#). Our model also employs an atmospheric-ocean heat transport parameterization that likely produces different model behavior during the transition between icy and warm climates than the static ocean assumption of [Turbet et al. \(2017\)](#). It is unclear how GCMs with fully-coupled atmospheric oceans may compare with the results presented here. This would be an interesting consideration for future studies.

We note that at low *CO₂* partial pressures surface *CO₂* condensation is more easily reached than what is qualitatively shown in [Figure 1](#). However, when planets are located far away enough from the host star and/or surface temperatures are low enough (such as for cold starts), *CO₂* condensation can easily take place during the evolution of the planet, once saturation pressure is reached. Some of the difference may be due to *H₂O* ice cloud warming that some GCMs predict in dry and cold atmospheres, but our model does not. An alternative reason for the differences may be in the spatial and vertical distributions of clouds, which are not accurately predicted by EBMs. Furthermore, the *CO₂* clouds formed in our simulations impact the planetary albedo, but they are non-absorbing (see [Section 2](#)). In contrast, the *CO₂* clouds of [Turbet et al. \(2017\)](#) are either radiatively active or inactive across the entire spectrum. Nevertheless, other GCM results are consistent with 1-D results (and, in turn, the EBM results here in the location of the outer edge of the habitable zone; [Wolf \(2018\)](#)). Our warm start results agree well with those predicted from 1-D radiative-convective climate models ([Kasting et al. 1993](#); [Kopparapu et al. 2013](#); [Ramirez 2018](#)).

Surface condensation of *CO₂* ice is highly dependent on the equator-to-pole temperature contrast, which in turn is sensitive to the diffusion coefficient *D* ([Equation 2](#)), which includes the planetary obliquity. We compared our results with those of past GCM simulations of snowball planets ([Hoffman et al. 2017](#)) to test the reliability of our diffusion parameterization. [Figure 6](#) shows the predicted latitudinally-averaged surface temperature distributions in our model. In general, our results agree quite well with the ones of [Hoffman et al. \(2017\)](#), lying near the lower range of surface temperatures, similar to the FOAM (Fast Ocean Atmosphere Model) model. Some of the GCM simulations are slightly warmer than ours (except for the FOAM model) because they predict the formation of highly-absorbing upper atmospheric *H₂O* ice clouds in these cold and (otherwise) dry atmospheres. More models should test this result. Nevertheless, we conclude that our employed heat diffusion parameterization is reasonable and consistent with previous studies.

In summary, the main differences between EBMs and GCMs are related to how large scale dynamics (which might lead to sharper climatic transitions) and clouds are treated, whose spatial and vertical distributions are not computed in most EBMs. In spite of that, our EBM exhibits latitudinal mean surface temperatures for Earth that are consistent with real-world data ([Ramirez & Levi 2018](#)). Our consistency with the GCM snowball simulations of [Hoffman et al. \(2017\)](#) is further suggestive of this. Furthermore, EBMs like

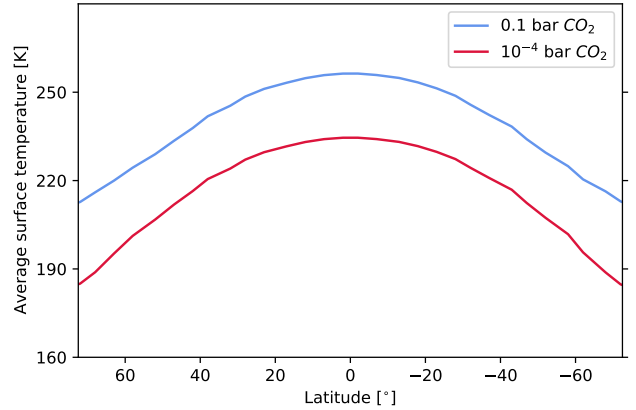


Figure 6. Average surface temperature as a function of latitude obtained using initial conditions corresponding to the GCM by [Hoffman et al. \(2017\)](#) ([Figure 8a](#)), for initial atmospheric *CO₂* contents of 0.11 mbar and 100 mbar. The surface albedo was set to 0.6 everywhere while planetary obliquity and eccentricity were set to 23.5° and zero, respectively.

the one presented here are computationally efficient, enabling the exploration of a wide parameter space, which would be computationally expensive with GCMs. Since this study mainly addresses different climatic trends and distributions, EBMs are appropriate tools. Ultimately, improved observations are needed to test how well climate models agree with reality, irrespective of complexity.

The habitable zone is the circumstellar region where standing bodies of liquid water could exist on the surface of a rocky planet ([Ramirez 2018](#)). In our solar system, a conservative estimate spans from ~0.95 - 1.67 AU ([Kasting et al. 1993](#); [Ramirez 2018](#)). Warm starts have traditionally been assumed in these and most other calculated habitable zone limits ([Kasting et al. 1993](#); [Pierrehumbert & Gaidos 2011](#); [Kopparapu et al. 2013](#); [Zsom et al. 2013](#); [Ramirez & Kaltenegger 2017](#); [Ramirez 2020](#)). In contrast, [Kadoya & Tajika \(2019\)](#) have shown that the habitable zone outer edge limit distance decreases for systems composed of cold start planets. Although that conclusion is consistent with the trends we find here for cold and warm start planets across all distances ([Figure 3](#)), we stress that a system’s outer edge limit corresponds to that for warm start planets should at least one such planet exist. In other words, without additional information regarding the planets themselves, the absolute outer edge limit in a stellar system is best characterized by its warm start limit (as computed previously) ([Kasting et al. 1993](#); [Kopparapu et al. 2013](#)).

We have compared our cold and warm start habitable zone limits with those of [Kadoya & Tajika \(2019\)](#), assuming the stellar properties outlined in [Table 2](#). For the Sun, [Kadoya & Tajika \(2019\)](#) obtain warm and cold start limits at ~ 1.69 and 1.49 AU, respectively, whereas corresponding limits for this study were found at ~ 1.68 and 1.39 AU. We attribute the slightly smaller cold start habitable zone limit (~ 7 % decrease) to differences in ice-albedo feedback parameterizations and in our addition of clouds, which are not included in their model. Likewise, their F-star warm and cold start limits are computed at ~ 3.2 and 2.75 AU whereas our F0 limits are located at ~ 3.1 and 2.62 AU, respectively. Therefore, the F0 values obtained here are smaller by about 3-5%. Again, our K5 warm and cold start limits are at ~ 0.74 and 0.65 AU, respectively, as compared to their K-star values at 0.73 and 0.66 AU. These are within 2% of each other and are overall consistent. We note that

any remaining differences with [Kadoya & Tajika \(2019\)](#) could be attributed to differences in the employed stellar spectra.

Similarly to [Kadoya & Tajika \(2019\)](#), we find that the difference in the stellar effective flux, S_{eff} , between cold and warm start distances decreases from hotter to cooler stars. Assuming $S_{\text{eff}} = 1$ is the incident energy received on Earth at 1 AU from the Sun, S_{eff} can be computed following [Kasting et al. \(1993\)](#) as

$$S_{\text{eff}} = \frac{L}{d^2}. \quad (5)$$

Here, L is stellar luminosity in solar units and d is the semi-major axis in astronomical units (AU). For instance, the solar S_{eff} from warm to cold starts increases by ~ 0.17 (i.e., from ~ 0.35 to 0.52), whereas this increase was only ~ 0.09 (from 0.27 to 0.36) for K5 stars. The S_{eff} increase was largest at ~ 0.18 (0.447 to 0.63) for the hotter (F0) stars. This trend occurs because the ice-albedo feedback weakens, whereas near-infrared absorption intensifies for habitable zone planets orbiting cooler stars, reducing the difference in S_{eff} between cold and warm start limits.

5 CONCLUSIONS

Planets similar to Earth might experience cold or warm stages during the course of their evolution. The carbonate-silicate cycle can stabilize planetary temperatures over geological timescales. While CO_2 generally increases the surface temperature, high enough atmospheric CO_2 can trigger atmospheric collapse via CO_2 surface ice condensation starting at the poles, potentially leading to irreversible glaciation. Such a process could negatively impact the habitability of terrestrial bodies, even if located within the canonical habitable zone. This was argued in [Turbet et al. \(2017\)](#), who showed that surface CO_2 ice condensation on initially frozen planets orbiting the Sun can significantly reduce the range of habitable orbital distances.

Our work confirms these results and extends the analysis to rapidly-rotating planets under different starting temperature conditions orbiting a range of star types (F - K). Using a latitudinally-dependent EBM, we show that planets that start out warm generally exhibit surface CO_2 ice condensation at significantly larger orbital distances than cold start (i.e., fully glaciated with $T_{\text{surf}} = 230$ K) planets. This implies a wide habitable zone, consistent with what had been previously computed using simpler 1-D models ([Kasting et al. 1993](#); [Kopparapu et al. 2013](#); [Ramirez 2018](#)). We also find that K-star planets are more resistant to atmospheric collapse than planets around larger stars. Finally, our heat diffusion parameterization provides a simple way of evaluating a range of warm and cold climates with minimal tuning of parameters.

The physics of planetary atmospheres remains complex, particularly for planets unlike the Earth. Future work should continue to use a hierarchy of models to explore the effects of clouds, convection, and the impact that oceans have on the overall heat transport.

ACKNOWLEDGEMENTS

I.B. acknowledges financial support from the Japanese Ministry of Education, Culture, Sports, Science and Technology (MEXT) and the Japanese Society for the Promotion of Science (JSPS). R.M.R. acknowledges funding from the Earth-Life Science Institute (ELSI) and from the National Institutes of Natural Sciences: Astrobiology Center (grant number JY310064). We thank the anonymous

reviewer for their constructive comments, which considerably improved the manuscript.

DATA AVAILABILITY

The code and the jupyter notebooks used for data analysis are available on Github at <https://github.com/irenebonati/CO2-condensation>.

REFERENCES

- Asolekar S., Valentine R., Schnoor J. L., 1991, *Water resources research*, 27, 527
- Batalha N. E., Kopparapu R. K., Haqq-Misra J., Kasting J. F., 2016, *Earth and Planetary Science Letters*, 455, 7
- Caballero R., Langen P. L., 2005, *Geophysical Research Letters*, 32, 1
- Forget F., Hourdin F., Talagrand O., 1998, *Icarus*, 131, 302
- Forget F., Wordsworth R., Millour E., Madeleine J.-B., Kerber L., Leconte J., Marcq E., Haberle R. M., 2013, *Icarus*, 222, 81
- Fray N., Schmitt B., 2009, *Planetary and Space Science*, 57, 2053
- Graham R., Pierrehumbert R., 2020, *Astrophysical Journal*, 896
- Haqq-Misra J., Kopparapu R. K., Batalha N. E., Harman C. E., Kasting J. F., 2016, *The Astrophysical Journal*, 827, 120
- Hayworth B. P. C., Kopparapu R. K., Haqq-Misra J., Batalha N. E., Payne R. C., Foley B. J., Ikwut-Ukwa M., Kasting J. F., 2020, *Icarus*, 345, 113770
- Hoffman P. F., Kaufman A. J., Halverson G. P., Schrag D. P., 1998, *Science*, 281, 1342
- Hoffman P. F., et al., 2017, *Science Advances*, 3, e1600983
- James P. B., North G. R., 1982, *Journal of Geophysical Research: Solid Earth*, 87, 10271
- Kadoya S., Tajika E., 2019, *The Astrophysical Journal*, 875, 7
- Kasting J. F., 1991, *Icarus*, 94, 1
- Kasting J. F., 2014, *Geological Society of America Special Papers*, 504, 19
- Kasting J. F., Whitmire D. P., Reynolds R. T., 1993, *Icarus*, 101, 108
- Kirschvink J. L., 1992, *Late Proterozoic low-latitude global glaciation: the snowball Earth*. Cambridge University Press
- Kite E. S., Mischna M. A., Gao P., Yung Y. L., Turbet M., 2020, *P&SS*, 181, 104820
- Kitzmann D., 2016, *The Astrophysical Journal Letters*, 817, L18
- Kopparapu R. K., et al., 2013, *The Astrophysical Journal*, 765, 131
- North G. R., Coakley Jr J. A., 1979, *Journal of the Atmospheric Sciences*, 36, 1189
- North G. R., Cahalan R. F., Coakley J. A., 1981, *Nasa-Cr-177133*
- Paradise A., Menou K., 2017, *The Astrophysical Journal*, 848, 33
- Pierrehumbert R. T., 2005, *Journal of Geophysical Research: Atmospheres*, 110
- Pierrehumbert R., Gaidos E., 2011, *The Astrophysical Journal Letters*, 734, L13
- Pierrehumbert R., Abbot D., Voigt A., Koll D., 2011, *Annual Review of Earth and Planetary Sciences*, 39, 417
- Ramirez R. M., 2017, *Icarus*, 297, 71
- Ramirez R. M., 2018, *Geosciences*, 8, 280
- Ramirez R. M., 2020, *Monthly Notices of the Royal Astronomical Society*, 494, 259
- Ramirez R. M., Kaltenecker L., 2017, *The Astrophysical Journal Letters*, 837, L4
- Ramirez R. M., Kaltenecker L., 2018, *The Astrophysical Journal*, 858, 72
- Ramirez R. M., Levi A., 2018, *Monthly Notices of the Royal Astronomical Society*, 4640, 4627
- Ramirez R. M., Kopparapu R., Zuger M. E., Robinson T. D., Freedman R., Kasting J. F., 2014, *Nature Geoscience*, 7, 59
- Ramirez R. M., Craddock R. A., Usui T., 2020, *Journal of Geophysical Research: Planets*, 125, e2019JE006160

- Rose B. E. J., Cronin T. W., Bitz C. M., 2017, *The Astrophysical Journal*, 846, 28
- Soto A., Mischna M., Schneider T., Lee C., Richardson M., 2015, *Icarus*, 250, 553
- Turbet M., Forget F., Leconte J., Charnay B., Tobie G., 2017, *Earth and Planetary Science Letters*, 476, 11
- Turbet M., Tran H., Pirali O., Forget F., Boulet C., Hartmann J.-M., 2019, *Icarus*, 321, 189
- Villanueva G., et al., 2015, *Science*, 348, 218
- Vladilo G., Murante G., Silva L., Provenzale A., Ferri G., Ragazzini G., 2013, *The Astrophysical Journal*, 767, 65
- Warren S. G., Wiscombe W. J., Firestone J. F., 1990, *Journal of Geophysical Research: Solid Earth*, 95, 14717
- Williams D. M., Kasting J. F., 1997, *Icarus*, 129, 254
- Williams D., Pollard D., 2003, *International Journal of Astrobiology - INT J ASTROBIOL*, 2
- Wolf E. T., 2018, *Astrophys. J. Lett*, 855
- Wordsworth R., Forget F., Selsis F., Madeleine J.-B., Millour E., Eymet V., 2010, *Astronomy & Astrophysics*, 522, A22
- Wordsworth R., Forget F., Millour E., Head J., Madeleine J.-B., Charnay B., 2013, *Icarus*, 222, 1
- Wordsworth R., Kalugina Y., Lokshtanov S., Vigasin A., Ehlmann B., Head J., Sanders C., Wang H., 2017, *Geophysical Research Letters*, 44, 665
- Xu K.-M., Krueger S. K., 1991, *Monthly weather review*, 119, 342
- Yang J., Abbot D. S., 2014, *The Astrophysical Journal*, 784, 155
- Zsom A., Seager S., De Wit J., Stamenković V., 2013, *The Astrophysical Journal*, 778, 109

This paper has been typeset from a $\text{\TeX}/\text{\LaTeX}$ file prepared by the author.